Physics Letters A 381 (2017) 524–528

Contents lists available at ScienceDirect

Physics Letters A

www.elsevier.com/locate/pla

Modulated exchange bias in NiFe/CoO/α-Fe_2O_3 trilayers and NiFe/CoO bilayers

X. Li [a], K.-W. Lin [b,*], W.-C. Yeh [b], R.D. Desautels [c], J. van Lierop [c,*], Philip W.T. Pong [a,*]

[a] Department of Electrical and Electronic Engineering, The University of Hong Kong, Hong Kong
[b] Department of Materials Science and Engineering, National Chung Hsing University, Taichung 402, Taiwan
[c] Department of Physics and Astronomy, University of Manitoba, Winnipeg, R3T2N2, Canada

ARTICLE INFO

Article history:
Received 1 November 2016
Accepted 23 November 2016
Available online 29 November 2016
Communicated by M. Wu

Keywords:
Nanomagnetics
Exchange bias
Magnetic thin film
Trilayer

ABSTRACT

While the exchange bias in ferromagnetic/antiferromagnetic (FM/AF) bilayer and FM1/AF/FM2 trilayer configurations has been widely investigated, the role of an AF2 layer in FM/AF1/AF2 trilayer configurations is still not well understood. In this work, the magnetic properties of NiFe/CoO, NiFe/α-Fe_2O_3 bilayers, and NiFe/CoO/α-Fe_2O_3 trilayer were studied comparatively. The microstructure and chemical composition were characterized. Temperature dependent magnetometry reveals increased irreversibility temperature in NiFe/CoO/α-Fe_2O_3 trilayer compared with NiFe/CoO bilayer. The magnetic hysteresis loops show that the exchange bias (H_{ex}) and coercivity (H_c) depend strongly on the anisotropy of AF layer (CoO, α-Fe_2O_3 and CoO/α-Fe_2O_3). Our work shows that the AF1/AF2 interfacial interactions can be used effectively for tuning the exchange bias in FM/AF1/AF2 trilayers.

1. Introduction

Exchange coupling is present in the pinned layers of various spintronic devices such as magnetic random access memories [1], magnetoresistive sensors [2], and spin torque oscillators [3]. When a ferromagnetic (FM) or ferrimagnetic (FI) layer is in contact with an antiferromagnetic (AF) layer, the magnetization of the FM can be pinned by the AF spins during the domain reversal processes [4–7], resulting in the field-shift of the magnetic hysteresis loops (H_{ex}) and the enhanced coercivity (H_c). Exchange bias is strongly influenced by the AF anisotropy [8]. The previous reports of various FM/AF bilayers have revealed that exchange bias can be controlled through adopting AF materials with different anisotropies such as CoO [9], NiO [10,11], MnO [12,13], MnPt [14], FeMn [15], and IrMn [16]. In addition, the AF spin structures can also be modified by engineering the structural and chemical composition [17,18], conducting ion-beam bombardment [19–21], or annealing under a magnetic field [22,23]. By contrast, the investigations of FM1/AF/FM2 trilayers [24–28] have revealed different exchange bias effects from those in bilayers. Unlike the conventional interpretation on the exchange bias in FM/AF bilayers where the exchange interaction is assumed to be an interfacial effect [29], recent investigations reveal that the exchange coupling of FM1/AF/FM2 trilayer can be largely influenced by the domain states in the bulk of AF [30–32]. On the other hand, both interfacial and interlayer interactions may contribute to the exchange coupling in FM/AF1/AF2 trilayers [33,34]. The interlayer coupling in $[IrMn/FeMn]_n$ super lattice is responsible for the tuned exchange bias, blocking temperature and thermal stability when interfacing with NiFe [35]. The research of NiFe/CoO/NiO trilayer has further revealed that the interlayer interaction is dominant when the thickness of CoO spacer is less than 3 nm [33,34]. This has inspired us to further explore the effect of AF1/AF2 interfacial coupling in FM/AF1/AF2 trilayer when a thick AF1 layer is engaged.

In the bulk, α-Fe_2O_3 is canted AF below $T_N = 948$ K with a small net magnetization due to the spin canting [36,37]. Spin reordering to a compensated AF occurs at 260 K, which is known as the Morin transition (T_M) [38]. In the present work, α-Fe_2O_3 is introduced as the third layer to modify the magnetic properties of a NiFe/CoO bilayer. The comparison of the magnetic properties of NiFe/CoO/α-Fe_2O_3, NiFe/CoO and NiFe/α-Fe_2O_3 at different temperatures provides insights into the exchange coupling in FM/AF1/AF2 trilayers.

2. Experimental methods

Trilayers of NiFe (24 nm)/CoO (12 nm)/α-Fe_2O_3 (12 nm) and bilayers of NiFe (24 nm)/CoO (12 nm) and of NiFe (24 nm)/α-Fe_2O_3 (12 nm) were prepared at ambient temperature using a dual ion-beam sputtering deposition technique [26,39]. The CoO was chosen

* Corresponding authors.
E-mail addresses: kwlin@dragon.nchu.edu.tw (K.-W. Lin), johan@physics.umanitoba.ca (J. van Lierop), ppong@eee.hku.hk (P.W.T. Pong).

http://dx.doi.org/10.1016/j.physleta.2016.11.033
0375-9601/

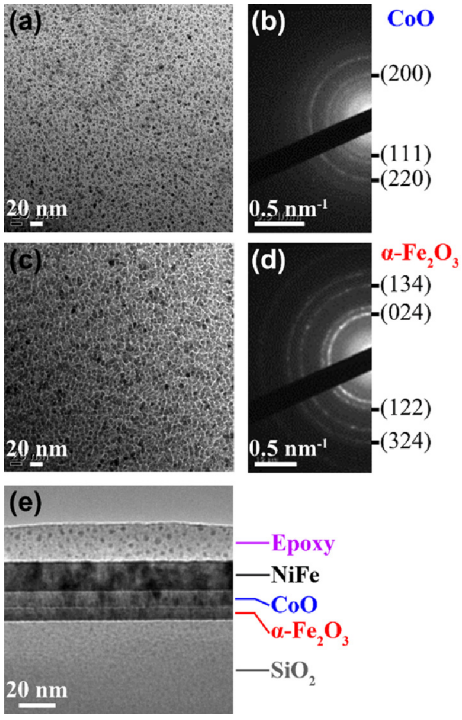

Fig. 1. The TEM images and electron diffraction patterns of (a), (b) CoO and (c), (d) α-Fe_2O_3 layers, and (e) the cross-sectional TEM image of NiFe/CoO/α-Fe_2O_3 trilayer.

to be relatively thick to reduce possible interlayer exchange coupling between NiFe and α-Fe_2O_3. During the deposition of the bottom Fe_2O_3 layer, a Kaufman ion source (800 V, 7.5 mA) was used to focus the argon ion beam onto a Fe target, while an End-Hall source with O_2/Ar ratios of 41% was used to in-situ oxidize the Fe. The CoO layer was prepared with O_2/Ar ratios of 8% O_2/Ar. The top NiFe layer was subsequently deposited by sputtering a $Ni_{80}Fe_{20}$ (at%) target with only the Kaufman source. An ULVAC-PHI X-ray photoelectron spectroscope (XPS, PHI 5000 Versa Probe) was used for the depth profile analysis and to identify the oxidation states. A JEOL (JEM-2010) transmission electron microscope (TEM) operating at 200 kV was used for the microstructural analysis. Magnetic properties were measured with a commercial vibrating sample magnetometer (ADE-DMS 1600 VSM) at room temperature, and a Quantum Design MPMS was used to measure the temperature-dependent magnetization and magnetic hysteresis at 10 K after 1.2 T in-plane field-cooling (FC) from 350 K.

3. Results and discussions

The microstructure of CoO, Fe_2O_3 single layer and NiFe/CoO/Fe_2O_3 trilayer was characterized by TEM (Fig. 1). Uniform polycrystalline surfaces with grain sizes ranging from 5 to 15 nm are observed in the CoO single layer sample (Fig. 1(a)). The Fe_2O_3 single layer presented columnar grains with diameter of ~10 nm (Fig. 1(c)). The CoO layer has a rock-salt structure with a lattice constant of 4.26 Å, as evidenced by the electron diffraction rings of CoO (111), (200), and (110) planes in Fig. 1(b). The formation of hexagonal α-Fe_2O_3 is also proved by the electron diffraction patterns in Fig. 1(d). The lattice constant is calculated to be 5.04 Å (the a-axis) and 13.75 Å (the c-axis). The cross-sectional TEM image (Fig. 1(e)) reveals the well-defined trilayer structure. The thin interfacial layers in NiFe/CoO and CoO/α-Fe_2O_3 are attributed to the diffusion through grain boundaries. The microstructures of NiFe, CoO and α-Fe_2O_3 layer are consistent with our previously reported NiFe/CoO [40,41] and NiFe/α-Fe_2O_3 bilayers [19,42].

The depth profile analysis by XPS of the NiFe/CoO/α-Fe_2O_3 trilayer (shown in Fig. 2(a)) reveals the oxidation states of Co and Fe in the middle CoO and bottom Fe_2O_3 layers, respectively. The sample surface is sputtered at ~0.25 nm/s while the XPS of Ni, Fe, Co, Si and O are characterized at 9 s intervals. The decrease in the oxygen signal with sputtering time ($t_{sp.}$) ≥0.2 min indicates that the naturally oxidized surface was sputtered away, whereas the increase in Ni and Fe signals suggests that the top layer is composed of metallic NiFe. When $t_{sp.}$ ≥1.6 min, the significant increase in the measured oxygen and cobalt intensity is attributed to the in-situ oxidation process from metallic Co into CoO during the deposition of the middle CoO layer. Also, at $t_{sp.}$ ≥2.8 min, the decrease in Co signal accompanied by the increase in Fe signal indicates that the bottom layer is composed of Fe_2O_3. Diffusion of Fe and Co in the NiFe/CoO layer is observed, as the defects and dislocations due to ion-beam bombardment act as diffusion paths. The intermixing may enhance the potential interfacial coupling between CoO and Fe_2O_3. For $t_{sp.}$ ≥3.5 min, the decline in Fe signal and the growth in both Si and O are consistent with the substrate being a thermally oxidized Si wafer. Further, XPS was used to distinguish the oxidation states of Co and Fe from the analysis of the core state shifts [43] of Co and Fe 2p states. At $t_{sp.}$ ~2.4 min, the two peaks positioned at binding energies of ~780 eV and ~796 eV correspond to the Co^{2+} (i.e., CoO) $2p_{3/2}$ and $2p_{1/2}$ states (accompanied with satellite peaks at ~786 eV and ~803 eV), respectively, as shown in Fig. 2(b). On the other hand, the oxidation state of Fe in the bottom Fe-oxide layer is determined to be Fe^{3+} (i.e., Fe_2O_3), as evidenced by the two peaks positioned at binding energies of ~710 eV ($2p_{3/2}$) and ~723 eV ($2p_{1/2}$) (Fig. 2(c)). The XPS analysis is qualitatively consistent with the microstructural results from TEM. These results indicate that the Fe atoms in Fe-oxide (41% O_2/Ar) were fully oxidized into α-Fe_2O_3 during the ion-beam bombardment due to the relatively high O_2/Ar ratio.

DC magnetometry (measured using a 10 mT field after zero-field-cooled (ZFC), and field-cooled (FC) processes) was used to examine the temperature-dependent magnetization of the NiFe coupled to the two different AF oxides (Fig. 3). The M_{FC} and M_{ZFC} branches recall those of an assembly of single-domain-sized NiFe crystallites that is resulted from the interplay between magnetic anisotropy and dipolar interactions [44] as evidenced by the "blocking" of the magnetization at lower temperatures (e.g. the convergence of M_{ZFC} and M_{FC} with warming from 10 K). For the NiFe/CoO bilayer (Fig. 3(a)), while the FC M vs. T scan exhibits typical $M_{FC}(T)$ behavior where the magnetization decreases with warming from 10 K to 400 K, the $M_{ZFC}(T)$ exhibits a maximum at the blocking temperature (T_B) of ~ 250 K. This indicates that the fluctuation of the spins of single-domain sized crystallites are frozen at temperatures below 250 K. In contrast, the NiFe/α-Fe_2O_3 bilayer exhibits much smaller T_B (70 ± 5 K) due to the smaller magnetocrystalline anisotropies (K) of α-Fe_2O_3 ($\sim 1.3 \times 10^5$ erg/cm^3 [42]) than CoO (5×10^5 erg/cm^3 [40]). The lower T_B compared with the bulk is believed to be resulted from the smaller crystallite size in the thin film. The irreversibility temperature (T_{irr}) is defined as the temperature where M_{ZFC} and M_{FC} curves diverge [45]. The low T_{irr} of 260 ± 5 K in NiFe/CoO bilayer indicates that the exchange bias emerges at temperatures below the Néel temperature of CoO ($T_{N,CoO} \sim 293$ K). This is possibly because of the finite thin film thickness and the disordered CoO domain structure due to ion-beam bombardment [46]. It is noted that the NiFe/CoO/α-Fe_2O_3 trilayer exhibits a compromised $T_{irr} = 250 \pm 5$ K compared with the NiFe/CoO bilayer ($T_{irr} = 260 \pm 5$ K) and NiFe/α-Fe_2O_3 bilayer ($T_{irr} = 70 \pm 5$ K). The modified T_{irr} of trilayer can be explained by the magnetic proximity effect [47] due to the interaction in CoO/α-Fe_2O_3. The coupling in CoO/α-Fe_2O_3 is

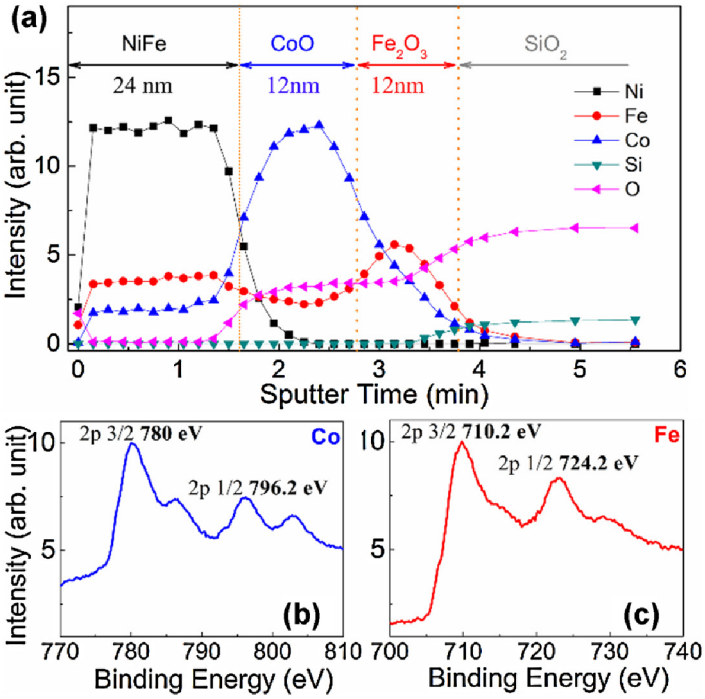

Fig. 2. (a) The depth profile and the binding energies of (b) Co and (c) Fe by XPS in a NiFe/CoO/Fe_2O_3 trilayer.

further enhanced by the field cooling from above the T_N of CoO [34]. This also indicates that the freezing behavior of the spins is modified by the CoO/α-Fe_2O_3 interaction.

To distinguish the different mechanisms in the FM NiFe layer that responds to an applied field due to coupling to different AF layers, the degree of divergence ($\Delta M_{\text{FC-ZFC}}$) [27] is shown in Fig. 3(b). The NiFe/α-Fe_2O_3 bilayer shows an increase in $\Delta M_{\text{FC-ZFC}}$ below T_{irr}. This indicates that the exchange coupling between NiFe and α-Fe_2O_3 dominates the magnetization reversal (e.g. reorienting with the applied field during the scan) for $T < 70$ K. However, the NiFe/CoO bilayer shows a broad magnetization plateau between ~ 50 K and 200 K before the further increase in $\Delta M_{\text{FC-ZFC}}$ at $T < 50$ K. The strength of exchange interaction can be quantitatively evaluated by ΔM at 10 K [12]. The larger $\Delta M_{\text{FC-ZFC}}$ in the NiFe/CoO bilayer (and NiFe/CoO/α-Fe_2O_3 trilayer) compared to the NiFe/α-Fe_2O_3 bilayer is attributed to the higher K in CoO compare with α-Fe_2O_3. These results indicate that the exchange coupling energy in FM/AF1 can also be tailored through AF1/AF2 interaction.

The hysteresis loops of the NiFe/CoO and NiFe/α-Fe_2O_3 bilayers, and the NiFe/CoO/α-Fe_2O_3 trilayer measured 180 K and 10 K are shown in Fig. 4 (a) and (b). The temperature dependence of $\mu_0 H_c$ and $\mu_0 H_{ex}$ are plotted in Fig. 4(c). At room temperature, all the samples exhibit coercivity of $\mu_0 H_c < 1$ mT (not shown here). After field cooling to 180 K, the phase transition of CoO into AF results in a significant shift ($\mu_0 H_{ex} = -12 \pm 1$ mT) and broadening ($\mu_0 H_c = 4 \pm 1$ mT) in hysteresis loop of NiFe/CoO bilayer (Fig. 4(a)). This is consistent with the $T_{irr} \sim 260$ K in NiFe/CoO bilayers shown in Fig. 3. The NiFe/α-Fe_2O_3 bilayer still exhibits small H_c and H_{ex}, as was reported previously [42]. This is resulted from the low T_{irr} ($\sim$70 K) as inferred from the M–T curve of NiFe/α-Fe_2O_3 bilayer. The NiFe/CoO/α-Fe_2O_3 trilayer has smaller $H_{ex}(\mu_0 H_{ex} = -10 \pm 1$ mT) and $H_c(\mu_0 H_c = 3 \pm 1$ mT) compared with the NiFe/CoO bilayer. The reduced H_{ex} can be attributed to the modified AF spin structure in CoO layer from exchange coupling to the net spins in α-Fe_2O_3. The AF layer forms a spiraling spin structure extending into the bulk when coupled with an FM layer during magnetization reversal [48]. The relative angle (θ) between the spins on the upper and bottom surfaces of a thick AF layer (>10 nm) could be 180° when sandwiched by two FM layers [49], while θ could be 0° in the FI/AF/FI trilayers [50]. It is possible that the AF layer may form a similar spiral-

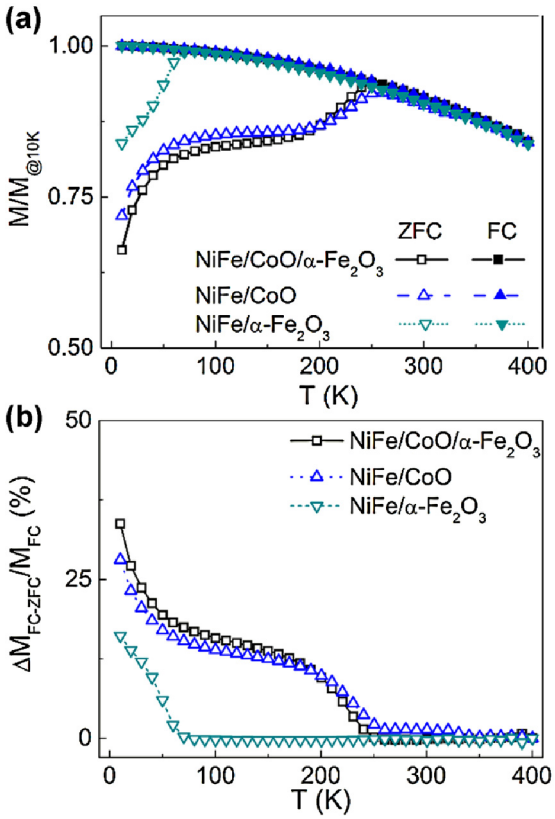

Fig. 3. The temperature dependence of (a) zero-field-cooled (ZFC) and field-cooled (FC) magnetization and (b) the difference in magnetization of NiFe/CoO and NiFe/α-Fe_2O_3 bilayers, and NiFe/CoO/α-Fe_2O_3 trilayers.

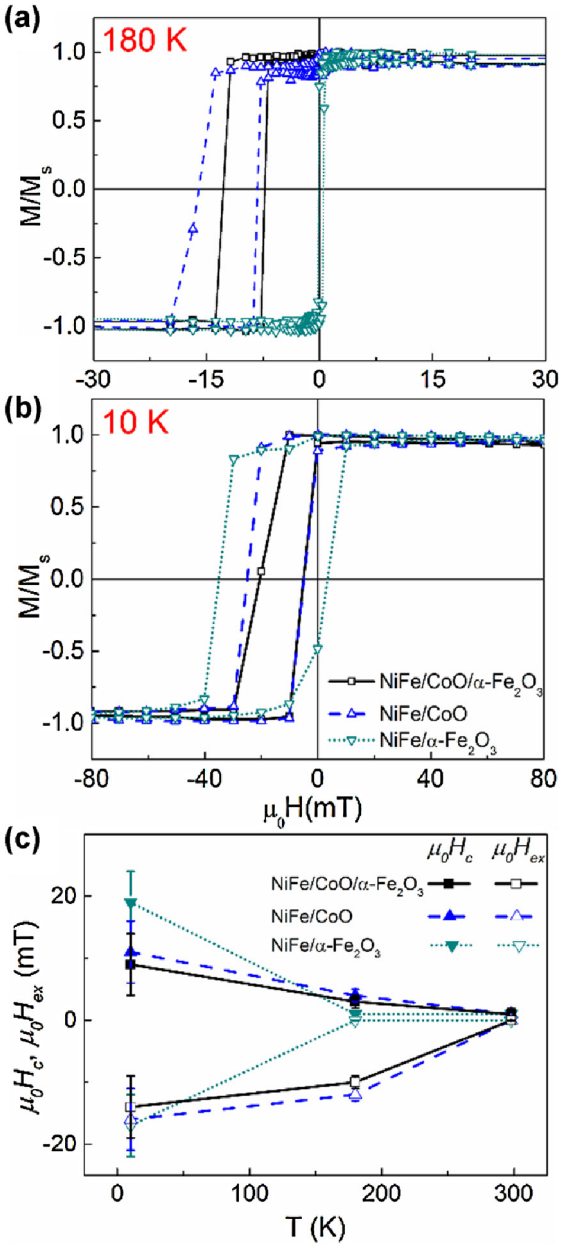

Fig. 4. The hysteresis loops of NiFe/CoO and NiFe/α-Fe_2O_3 bilayers, and NiFe/CoO/α-Fe_2O_3 trilayers measured at (a) 180 K and (b) 10 K after field cooling in 1.2 T in the film plane from 350 K, and (c) the temperature dependence of $\mu_0 H_c$ and $\mu_0 H_{ex}$.

ing spin structure with $\theta < 180°$ in the NiFe/CoO/α-Fe_2O_3 trilayer. During magnetization reversal, the α-Fe_2O_3 affects the spin structure of CoO by accelerating the domain nucleation and growth [51], resulting in the smaller H_{ex} in trilayer. At 10 K, the superparamagnetic-sized single domain crystallites in α-Fe_2O_3 are blocked and "drag" the adjacent NiFe crystallites during reversal, resulting in evident loop shift ($\mu_0 H_{ex} = -17 \pm 5$ mT) and enhanced H_c ($\mu_0 H_c = 19 \pm 5$ mT) in NiFe/α-Fe_2O_3 bilayer (Fig. 4(b)). The larger H_{ex} and H_c in NiFe/α-Fe_2O_3 bilayer compared with NiFe/CoO bilayer ($\mu_0 H_{ex} = -16 \pm 5$ mT and $\mu_0 H_c = 11 \pm 5$ mT) indicate that the high NiFe/Fe_2O_3 exchange coupling constant ($A = 6 \times 10^{-5}$ erg/cm^2 [42]) dominates the exchange bias in contact with the NiFe layer (since H_{ex} is proportional to $\sqrt{AK}$). Compared with the NiFe/CoO bilayer, the NiFe/CoO/α-Fe_2O_3 trilayer presents no obvious reduction in H_{ex} and H_c (cf. $\mu_0 H_{ex} = -14 \pm 5$ mT and $\mu_0 H_c = 9 \pm 5$ mT) considering the uncertainties of measurement. At low temperatures, the interfacial exchange coupling in NiFe/CoO is reported to be enhanced [27]. On the other hand, the disappearance of the net spins in α-Fe_2O_3 due to the Morin transition may also result in weaker coupling in CoO/α-Fe_2O_3, which reduces the modification effect on bulk spins in CoO layer. The small difference between the H_{ex} of the trilayer and NiFe/CoO bilayer is believed to be resulted from the enhanced NiFe/CoO coupling and suppressed CoO/α-Fe_2O_3 coupling.

4. Conclusions

The exchange coupling in NiFe/CoO, NiFe/α-Fe_2O_3 bilayers, and NiFe/CoO/α-Fe_2O_3 trilayers were studied. Uniform CoO grains and nanocolumnar α-Fe_2O_3 grains were characterized by TEM. DC magnetometry results revealed shifted T_{irr} in NiFe/CoO/α-Fe_2O_3 trilayer compared with the NiFe/CoO bilayer. At room temperature, all samples showed low H_c. After field cooling to 180 K, the NiFe/CoO/α-Fe_2O_3 trilayer exhibited smaller H_{ex} and H_c than the NiFe/CoO bilayer, possibly because the spiraling spin structures in CoO were modified through coupling to the AF α-Fe_2O_3 in trilayers. At 10 K, the blocking of α-Fe_2O_3 crystallites resulted in remarkably enhanced H_{ex} and H_c in NiFe/α-Fe_2O_3. The H_{ex} and H_c of NiFe/CoO/α-Fe_2O_3 trilayer showed no obvious change compared with NiFe/CoO bilayer. This work shows that the interfacial exchange coupling in thick AF1/AF2 bilayers also modifies the exchange coupling to the adjacent FM layer. These results have provided a novel approach to tailor the magnetic properties of FM/AF layers through interfacing with the antiferromagnetic third layer.

Acknowledgements

This work was supported by the MOST of Taiwan, NSERC and CFI of Canada, Seed Funding Program for Basic Research, Seed Funding Program for Applied Research and Small Project Funding Program from the University of Hong Kong, ITF Tier 3 funding (ITS-104/13, ITS-214/14), and University Grants Committee of HK (AoE/P-04/08).

References

[1] C. Chappert, A. Fert, F.N. Van Dau, Nat. Mater. 6 (2007) 813–823.
[2] P.A. Grünberg, Rev. Mod. Phys. 80 (2008) 1531–1540.
[3] A.M. Deac, A. Fukushima, H. Kubota, H. Maehara, Y. Suzuki, S. Yuasa, Y. Nagamine, K. Tsunekawa, D.D. Djayaprawira, N. Watanabe, Nat. Phys. 4 (2008) 803–809.
[4] W.H. Meiklejohn, J. Appl. Phys. 29 (1958) 454–455.
[5] J. Nogués, J. Sort, V. Langlais, V. Skumryev, S. Suriñach, J.S. Muñoz, M.D. Baró, Phys. Rep. 422 (2005) 65–117.
[6] R.L. Stamps, J. Phys. D, Appl. Phys. 33 (2000) R247–R268.
[7] K. O'Grady, L.E. Fernandez-Outon, G. Vallejo-Fernandez, J. Magn. Magn. Mater. 322 (2010) 883–899.
[8] A.E. Berkowitz, K. Takano, J. Magn. Magn. Mater. 200 (1999) 552.
[9] K. Takano, R.H. Kodama, A.E. Berkowitz, W. Cao, G. Thomas, Phys. Rev. B 79 (1997) 1130.
[10] D.-H. Han, J.-G. Zhu, J.H. Judy, J. Appl. Phys. 81 (1997) 4996–4998.
[11] D.L. Cortie, C. Shueh, B.C. Lai, P.W.T. Pong, J. van Lierop, F. Klose, K.W. Lin, IEEE Trans. Magn. 50 (2014) 1–4.
[12] K.-W. Lin, C. Shueh, C.-H. Liu, E. Skoropata, T.-H. Wu, J. van Lierop, J. Appl. Phys. 113 (2013) 17C104.
[13] A.C. Sun, H.F. Hsu, H.J. Wu, J.H. Hsu, P.W.T. Pong, T. Suzuki, K.W. Lin, IEEE Trans. Magn. 47 (2011) 501.
[14] M. Rickart, A. Guedes, B. Negulescu, J. Ventura, J.B. Sousa, P. Diaz, M. MacKenzie, J.N. Chapman, P.P. Freitas, Eur. Phys. J. B 45 (2005) 207–212.
[15] X.-L. Tang, H.-W. Zhang, H. Su, Z.-Y. Zhong, Y.-L. Jing, J. Magn. Magn. Mater. 312 (2007) 366–369.
[16] A. Kovacs, A. Kohn, J. Dean, T. Schrefl, A. Zeltser, M.J. Carey, IEEE Trans. Magn. 45 (2009) 3873–3876.
[17] X. Li, K.W. Lin, H.Y. Liu, D.H. Wei, G.J. Li, P.W.T. Pong, Thin Solid Films 570 (2014) 383–389.
[18] K.-W. Lin, J.-Y. Guo, J. Appl. Phys. 104 (2008) 123913.
[19] C. Zheng, T.-C. Lan, C. Shueh, R.D. Desautels, J. van Lierop, K.-W. Lin, P.W.T. Pong, Jpn. J. Appl. Phys. 53 (2014) 06JB03.

[20] K.W. Lin, T.J. Chen, J.Y. Guo, H. Ouyang, D.H. Wei, J. Van Lierop, J. Appl. Phys. 105 (2009) 07D710.
[21] G. Li, C.W. Leung, C. Shueh, H.-F. Hsu, H.-R. Huang, K.-W. Lin, P.T. Lai, P.W.T. Pong, Surf. Coat. Technol. 228 (2013) S437–S441.
[22] G. Li, C.W. Leung, Y.-J. Wu, A.-C. Sun, J.H. Hsu, P.T. Lai, K.-W. Lin, P.W.T. Pong, Microelectron. Eng. 110 (2013) 250–255.
[23] G. Li, C.W. Leung, Y.-C. Chen, K.-W. Lin, A.-C. Sun, J.-H. Hsu, P.W.T. Pong, Microelectron. Eng. 110 (2013) 241.
[24] P.G. Barreto, M.A. Sousa, F. Pelegrini, W. Alayo, F.J. Litterst, E. Baggio-Saitovitch, Appl. Phys. Lett. 104 (2014) 202403.
[25] X.H. Liu, W. Liu, S. Guo, F. Yang, X.K. Lv, W.J. Gong, Z.D. Zhang, Appl. Phys. Lett. 96 (2010) 082501.
[26] D.L. Cortie, Y.-W. Ting, P.-S. Chen, X. Tan, K.-W. Lin, F. Klose, J. Appl. Phys. 115 (2014) 073901.
[27] K.-W. Lin, T.-C. Lan, C. Shueh, E. Skoropata, J. van Lierop, J. Appl. Phys. 115 (2014) 17D717.
[28] C.W. Leung, M.G. Blamire, Phys. Rev. B 72 (2005) 054429.
[29] W.H. Meiklejohn, J. Appl. Phys. 33 (1962) 1328–1335.
[30] R. Morales, Z.-P. Li, J. Olamit, K. Liu, J.M. Alameda, I.K. Schuller, Phys. Rev. Lett. 102 (2009) 097201.
[31] P. Miltényi, M. Gierlings, J. Keller, B. Beschoten, G. Güntherodt, U. Nowak, K.D. Usadel, Phys. Rev. Lett. 84 (2000) 4224–4227.
[32] M.Y. Khan, C.-B. Wu, W. Kuch, Phys. Rev. B 89 (2014) 094427.
[33] M.J. Carey, A.E. Berkowitz, J.A. Borchers, R.W. Erwin, Phys. Rev. B 47 (1993) 9952–9955.
[34] M.J. Carey, A.E. Berkowitz, J. Appl. Phys. 73 (1993) 6892–6897.
[35] K. Akmaldinov, C. Ducruet, C. Portemont, I. Joumard, I.L. Prejbeanu, B. Dieny, V. Baltz, J. Appl. Phys. 115 (2014) 17B718.
[36] A.H. Morrish, Canted Antiferromagnetism: Hematite, World Scientific, Singapore, 1994.
[37] H.J. Williams, R.C. Sherwood, J.P. Remeika, J. Appl. Phys. 29 (1958) 1772–1773.
[38] H.S. Nabi, R.J. Harrison, R. Pentcheva, Phys. Rev. B 81 (2010) 214432.
[39] R. Magaraggia, M. Kostylev, R.L. Stamps, K.W. Lin, J.Y. Guo, K.J. Yang, R.D. Desautels, J. van Lierop, IEEE Trans. Magn. 47 (2011) 1614–1618.
[40] J. van Lierop, B.W. Southern, K.W. Lin, Z.Y. Guo, C.L. Harland, R.A. Rosenberg, J.W. Freeland, Phys. Rev. B 76 (2007) 224432.
[41] K.W. Lin, F.T. Lin, Y.M. Tzeng, Z.Y. Guo, Eur. Phys. J. B 45 (2005) 237.
[42] J. van Lierop, K.-W. Lin, Z.-Y. Guo, P.-H. Ko, H. Ouyang, J. Appl. Phys. 101 (2007) 09E505.
[43] K.-W. Lin, F.-T. Lin, Y.-M. Tzeng, IEEE Trans. Magn. 41 (2005) 927–929.
[44] S. Laureti, S.Y. Suck, H. Haas, E. Prestat, O. Bourgeois, D. Givord, Phys. Rev. Lett. 108 (2012) 077205.
[45] P. Zhang, F. Zuo, F.K. Urban III, A. Khabari, P. Griffiths, A. Hosseini-Tehrani, J. Magn. Magn. Mater. 225 (2001) 337–345.
[46] I.O. Dzhun, S.A. Dushenko, N.G. Chechenin, E.A. Konstantinova, J. Phys. Conf. Ser. 303 (2011) 012103.
[47] P.K. Manna, S.M. Yusuf, Phys. Rep. 535 (2014) 61–99.
[48] M.D. Stiles, R.D. McMichael, Phys. Rev. B 59 (1999) 3722–3733.
[49] F.Y. Yang, C.L. Chien, Phys. Rev. Lett. 85 (2000) 2597–2600.
[50] P.A.A. van der Heijden, C.H.W. Swüste, W.J.M. de Jonge, J.M. Gaines, J.T.W.M. van Eemeren, K.M. Schep, Phys. Rev. Lett. 82 (1999) 1020–1023.
[51] V. Nikitenko, V. Gornakov, L. Dedukh, Y.P. Kabanov, A. Khapikov, A. Shapiro, R. Shull, A. Chaiken, R. Michel, Phys. Rev. B 57 (1998) R8111.